[Research Paper] 대한금속 · 재료학회지 (*Korean J. Met. Mater.*), Vol. 59, No. 8 (2021) pp.567-574
DOI: 10.3365/KJMM.2021.59.8.567

A Study on the Effects of Surface Energy and Topography on the Adhesive Bonding of Aluminum Alloy

Gilho Kang* and Wonjong Choi

Department of Materials Engineering, Korea Aerospace University, Gyeonggi-do 10540, Republic of Korea

Abstract: The bonding properties of adhesives are mainly affected by surface roughness, topography and chemical adsorption. In this paper, we studied the effects of surface pretreatment of Al 2024-T3 (bare) in terms of surface roughness, topography and surface free energy. Surface pre-treatment included solvent cleaning, FPL etching, PAA and CAA treatment. The surface energy and roughness of the aluminum surface were significantly increased by the anodizing treatment. Single lap shear and fatigue tests were performed to investigate bonding properties and durability. The evaluation revealed that the surface energy and surface roughness resulting from the aluminum surface treatment had a significant impact on bonding properties and durability. PAA treated surfaces had the highest bonding strength, and CAA treated surfaces had superior bonding retention performance in hot water or salt spray environments. The results of the fatigue test most clearly demonstrated how the surface pretreatment of the aluminum alloy differently affected bonding performance.

(Received March 27, 2021; Accepted May 10, 2021)

Keywords: adhesive, bonding strength, anodizing, surface roughness

1. Introduction

Bond strength and durability depend on the type of interaction between the adhesive and the adherend. The type of interaction depends upon the chemical makeup of the adhesives and adherends and also the topography of the adherend surface [1-3]. Adhesion can be improved by mechanically removing the weak surface layer, increasing the substrate surface roughness, surface area and wettability, and improving the energy dissipation mechanism of the adhesive. There is no universal adhesion model that accurately describes the bonding properties of various bonded joints, the various combinations of attachments as well as adhesives exposed to various environments. Almost all adhesion models can be grouped into five major adhesion theories – the mechanical interlocking theory, chemical/adsorption theory, diffusion theory, electrical theory and weak boundary layer theory [4,5].

Mechanical interlocking is a major contributing factor in the adhesion of polymers, metals and other materials [6-8]. The adherend surface is mechanically or chemically treated to obtain the desired porosity and rough adherend surface morphology. Chemical treatments involve polishing, etching, anodizing and other special treatments such as plasma and laser techniques [9-18]. Studies have shown that a two-stage polarization process can increase surface porosity and roughness [19]. Mechanical treatments usually involve scrubbing and polishing with sandpaper and grit blasting. Adhesion via mechanical interlocking requires that the adhesive penetrates the geometric irregularities of the adherend surface. Hennemann and Brockmann provided evidence of penetration of thermoset adhesives into the pores of anodized oxide [20]. The degree to which the polymer penetrates into the oxide pores depends on the wettability of the surface and the shape of the pores. The chemical/adsorption properties between the adhesive and adherend are also important for adhesion. These include the energy of adhesion in terms of the surface energy of the materials. Joannie W. Chin *et al*. measured the surface energy and chemistry of a toughened BMI composite where the surface was pretreated via solvent wiping, peeling, plying, grit-

-
**Corresponding Author:*
[Tel: +82-, E-mail:]

blistering and oxygen plasma. They subsequently facilitated a comparison using double lap shear and wedge tests [21]. Kunio Uehara and Mitsuru Sakurai studied bonding strength in relation to the surface roughness of the joining parts. They concluded that an optimum surface roughness (3~6 μm) existed in determining the tensile strength of the adhesion, and the curve trend showing the relationship between bond strength and surface roughness could be explained by considering three factors: (1) the strength based on the adhesion theory (2) the surface area effect (3) the notch effect due to surface roughness [22].

The purpose of this study is to clarify the impact of the surface treatment of an aluminum adherend, from the aspects of micro-roughness and surface energy. The surface treatment of the aluminum involved solvent wiping, Forest Products Laboratory (FPL) etching, phosphoric acid anodizing (PPA) and chromic acid anodizing (CAA). Single lap-shear and fatigue tests were performed to compare the adhesion properties for each pretreated surface.

2. Experiment

2.1 Materials

Cytec FM 300M epoxy-based film adhesive, widely used to bond metal to metal, metal to composite, and metal to honeycomb, was used. FM 300M adhesive film has a high level of elongation and toughness along with high ultimate shear strength, which is particularly suitable for redistributing the high shear stress concentration of graphite epoxy-to-metal bonds and can accommodate the low interlaminar shear strength of composites [23]. It has excellent fatigue resistance in these joints. Tricot carriers, tightly woven in properly designed and machined joints, provide a certain level of electrical insulation between the metal and graphite composites to reduce galvanic corrosion. 1.6-mm thick bare Al 2024-T3 (Alcore, Inc.) was used for the adherend.

2.2 Surface pretreatment

A summary of the surface treatment is presented in Table 1. The aluminum surface cleaning consisted of ultrasonic cleaning for 5 min in an acetone solution followed by rinsing with distilled water and then drying at 60 ºC.

FPL etching is a common chemical method that provides a rough surface for bonding. It uses a mixture of sodium dichromate and sulfuric acid, and can be used as a standalone pretreatment for bonding or in conjunction with an anodizing process. The specification covering FPL etching is ASTM D 2674-72. The FPL etching procedure is as follows. The aluminum surface was degreased in both vapor and hot liquid 1,1,1-trichloroethane for 4 min at 88 ºC. Alkaline cleaning was carried out for 13 min at 50 ºC and was then rinsed for 4 min at room temperature. The FPL etching process was carried out for 13 min at 63 ºC and was then rinsed for 5 min at 23 ºC. Finally, it was dried at 60 ºC. In addition to etching, some coupons were also anodized in phosphoric acid for 23min at 23 ºC, 15 V and 1500A.

Table 1. Surface pretreatment summary

Pretreatment	Process description
1. Cleaning	Ultrasonic cleaning within acetone
2. FPL etching	Vapor degreasing, alkaline cleaning, FPL etching
3. PAA (Phosphoric Acid Anodizing)	FPL etching, PAA
4. CAA (Chromic Acid Anodizing)	HNO_3 etching, CAA, sealing

Another anodizing pretreatment was carried out in a chromic acid solution for 35 min at 34 ºC, 22V and 2000A. After the chromic acid anodizing treatment, it was sealed in a dilute chromate solution for 25 min at 90 ºC.

2.3 Surface energy measurement

Surface free energy (γ) generally consists of a dispersion component (γ^D) and a polar component (γ^P), which arise from two types of intermolecular forces, dispersion and polar, as shown by

$$\gamma = \gamma^D + \gamma^P$$

The surface tension leading to the formation of the angle is pictured in Fig. 1.

This relationship was described by Young in 1805, resulting in the following well known expression:

$$\gamma_{SV} = \gamma_{SL} + \gamma_{LV} \cos\theta + \pi_e$$

π_e is the spreading pressure, which turns out to be

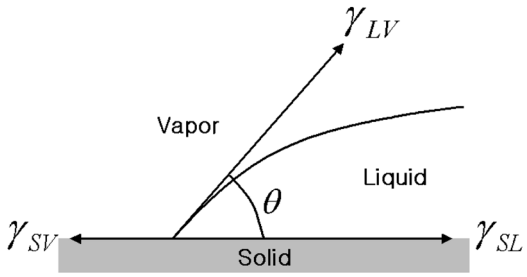

Fig. 1. Layout of the interface of a liquid droplet on a solid surface

negligible in liquids where the contact angle of the polymer surface is not zero. The interfacial tension between the solid and the liquid was obtained using the geometric-mean method as

$$\gamma_{SL} = \gamma_{SV} + \gamma_{LV} - 2\sqrt{\gamma_{SV}^{P}\gamma_{LV}^{P}} - 2\sqrt{\gamma_{SV}^{D}\gamma_{LV}^{D}}$$

Combining the above two equations and neglecting the spreading pressure gives [24].

$$\gamma_{LV}(1 + \cos\theta) = 2\sqrt{\gamma_{SV}^{P}\gamma_{LV}^{P}} + 2\sqrt{\gamma_{SV}^{D}\gamma_{LV}^{D}}$$

We calculated the surface energy of the aluminum using the Young-Depre relationship from two liquids for which the surface energy is known. We used water and diiodomethane. For the water, the values of γ_{SV}^{D} and γ_{SV}^{P} used in the calculation were 51 and 21.8. For the diiodomethane, the values of γ_{SV}^{D} and γ_{SV}^{P} were 50.42 and 0.38 [25]. A Sigma 70 (KSV surface tensiometer) was employed to carry this out.

The work of adhesion, W_A, in turn is defined as the energy per unit area of the interaction between the liquid and solid:

$$W_A = \gamma_{SV} + \gamma_{LV} - \gamma_{SL}$$

Eliminating Y_{SL} from the combined Young equation enabled the Young-Dupre relationship to be determined, as follows

$$W_A = \gamma_{LV}(1 + \cos\theta)$$

According to Owens and Wendt's geometric approach, the work of adhesion, W_A, between the solid and liquid is equal to the sum of the dispersive and polar interactions [26,27].

$$W_A = W_A^D + W_A^P, \text{ and } W_A = 2\sqrt{\gamma_{LV}^{D}\gamma_{SV}^{D}} + 2\sqrt{\gamma_{LV}^{P}\gamma_{SV}^{P}}$$

The roughness correction factor had to be calculated because the difference in surface roughness can change the measured contact angle and affect subsequent surface energy calculations [21]. Samples and a smooth slide-glass plate were coated with approximately 50 nm of gold in a sputter coater. The slide-glass plate served as a reference smooth surface. The contact angles of 10 drops of liquid were measured on the gold-coated samples as well as the gold-coated slide-glass plate. A roughness correction factor, R_C was calculated via

$$R_C = \frac{\cos\theta_{sample}}{\cos\theta_{glass\ plate}}$$

where θ is the contact angle of a liquid with a known surface energy. These roughness correction factors (R_C) were used to correct the contact angle values of various pretreatment substrate surfaces.

2.4 Surface roughness measurement

Surface analysis was performed to confirm the changes introduced to the Al substrate by the various pretreatments. An SE1700α laser scanning microscope (LSM) (Carl Zeiss Alpha 7) and SPM-400 atomic force microscope (AFM) (Seiko Instruments) were used to study the surface roughness and topography, respectively. The scanning length differed for each measuring instrument because the resolution of each system was very different. Several areas on each sample were scanned at widths of 0.3 μm by 0.3 μm and 1 μm by 1 μm using AFM. From the LSM, scanning widths of 6 μm by 6 μm, 60 μm by 60 μm and 1000 μm by 1000 μm were used. For the SE1700α, the scanning length of the surface was 4 mm. We compared the roughness of each different surface with the scanning length.

The root mean square (RMS) (R_a), average roughness (R_z) and S_{ratio} were measured and compared using the AFM. The average roughness was the area between the roughness profile and its mean line, or the integral of the absolute value of the roughness profile height over the evaluation length.

$$R_a = \frac{1}{L}\int_0^L |r(x)|dx$$

The RMS roughness of a surface was calculated from another integral of the roughness profile.

$$RMS = \sqrt{\frac{1}{L}\int_0^L r^2(x)dx}$$

R_z (ISO) is a parameter that averages the height of the 5 highest peaks and the depth of the 5 deepest valleys over the evaluation length. S_{ratio} was calculated by

$$S_{ratio} = \frac{A_M}{A_F}$$

A_M: measured surface area from AFM

A_F: measured flat area

2.5 Bonding properties

Single lap-shear (SLS) test coupon profiles of the rectangular cross-section with a thickness of 1.6 mm and width of 25.4 mm were cut at 101.6 mm, and lap shear joints were produced with a 12.7-mm bond overlap according to ASTM D1002. The specimens that were bonded with the film adhesive were completely cured and bonded at 175 ºC for 60 min in an autoclave at 276 kPa.

The specimens were immersed in water at 70 ºC for 60 days, and some specimens were tested under salt spray conditions (5% NaCl, 200 hr.) using a salt spray tester (SUGA, Model ST90). The lap-shear strength was subsequently measured at a test speed of 1.3 mm/min.

The specimen's geometry of fatigue tests was identical to the SLS test. Fatigue tests were performed on an Instron servohydraulic machine in constant amplitude load. All fatigue tests were conducted at room temperature with a stress ratio of 0.5, a maximum load of 500 kgf and a tension of 30 Hz.

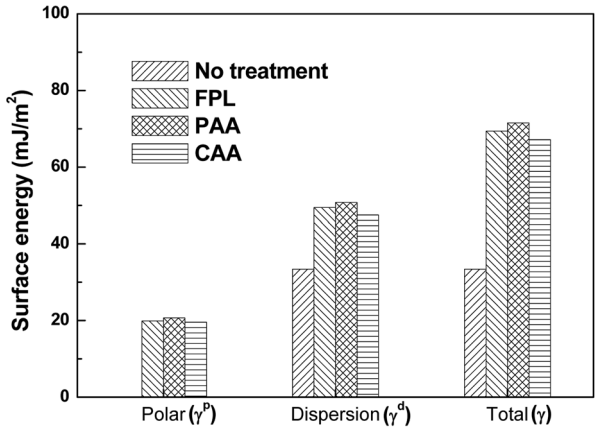

Fig. 2. Surface energy of each pretreated aluminum alloy (2024-T3) surface

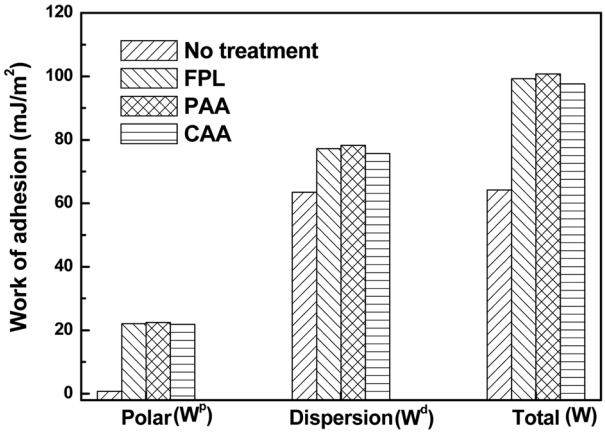

Fig. 3. Work of adhesion of each pretreated aluminum alloy (2024-T3) surface

3. RESULTS AND DISCUSSION

3.1 Surface free energy

The surface energy and the work of adhesion (W_A) for each pretreated aluminum surface are shown in Figs. 2 and 3, respectively. The polarity component of the cleaned aluminum surface was almost zero, but after FPL etching and anodizing, it rose to about 20 mJ/m^2. The PAA treated surface had the highest surface energy and work of adhesion. However, this was a result of not considering the effects of surface roughness. The roughness correction factor for each surface condition was measured relative to the slide-glass plate. The roughness factor (R_c) was taken to be 1.0 for the slide-glass plate. The roughness factor of each treated aluminum surface is shown in Table 2. Following the cleaning and CAA treatment, the roughness factor was about the same as that of the glass plate, and the PAA treated surface showed the highest roughness factor. The surface energy and work of adhesion, after taking into account the correction factor, are shown in Figs. 4~5, respectively. In this case, the CAA treated surface had the highest polarity, surface energy and

Table 2. The roughness correction factor of each treated aluminum surface

Surface	Contact angle (degree)	Correction factor
Glass plate	87.43	1
Cleaning	86.9	1.2
FPL	75.34	5.6
PAA	40.45	16.9
CAA	87.58	0.9

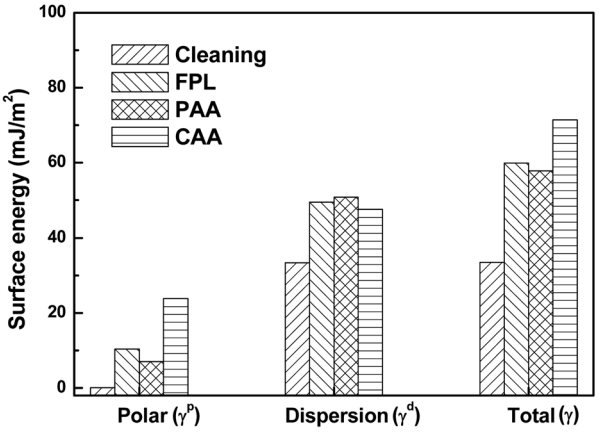

Fig. 4. Surface energy considering roughness correction factor

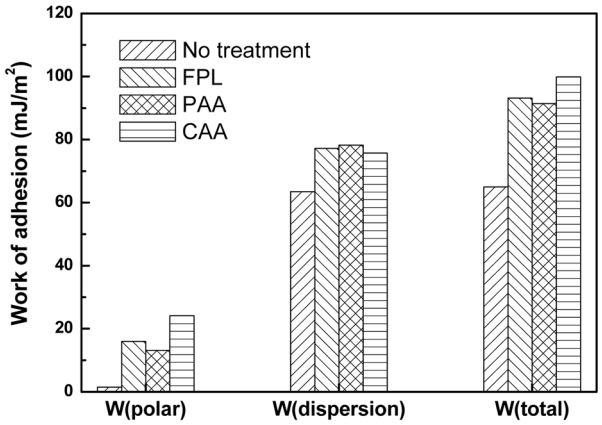

Fig. 5. Work of adhesion considering roughness correction factor

work of adhesion.

3.2 Surface roughness

The surface roughness is an important parameter in adhesive bonding. The average roughness (R_a) of each pretreated aluminum surface along the scanned length is shown in Fig. 6. The smaller the scanning length, the larger the difference in surface roughness. The difference in surface roughness was noticeable when the scanning length was 0.3 μm. The scanning image from the AFM is shown in Fig. 7. The anodized surface had a regular cell structure, while the cleaned surface had an irregular shape. From this image, the cell size of the PAA treated surface was about 35 to 45 nm. The cell structure of the CAA treated surface was finer because this surface was finally sealed. Sealing is usually completed by reacting the CAA surface with hot water. Hydrous oxides produced from this process fill the pores and make an impermeable anodized layer that is stable in a wide range of atmospheric and environmental conditions.

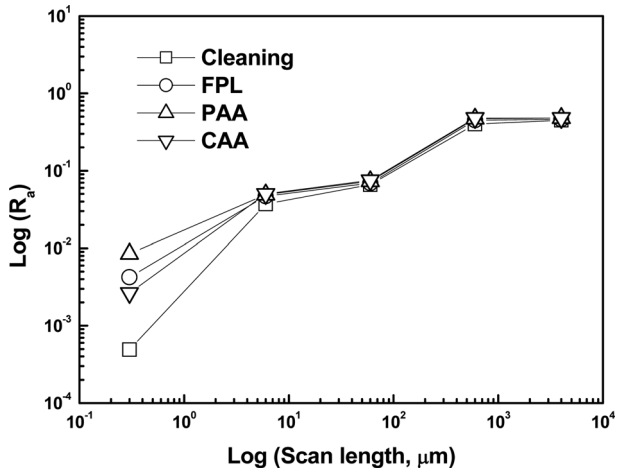

Fig. 6. Average roughness of each pretreated aluminum alloy along scanned length

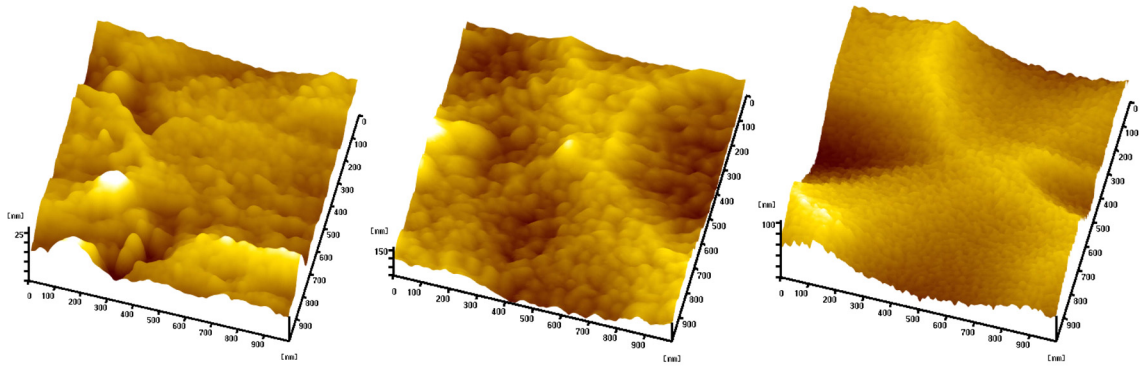

Fig. 7. AFM images showing each surface pretreatment; (a) Cleaning (b) PAA and (c) CAA

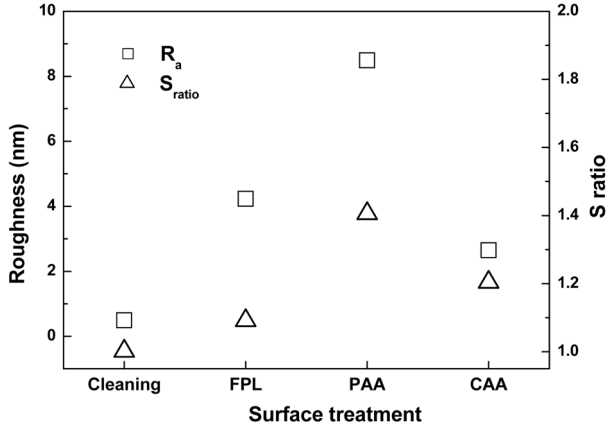

Fig. 8. Average roughness and S ratio of each pretreated aluminum alloy

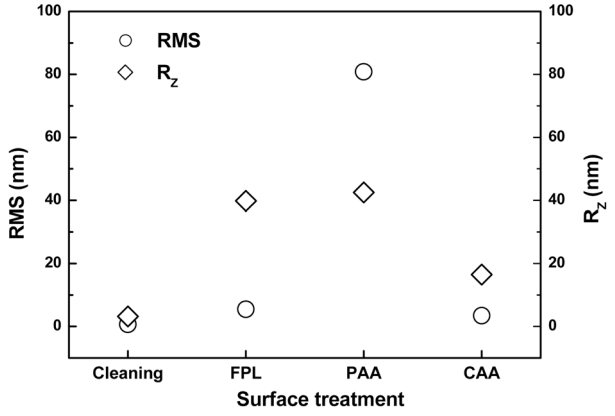

Fig. 9. RMS and Rz of each pretreated aluminum alloy

The R_a, S_{ratio}, RMS and R_z values from the AFM are shown in Figs. 8 and 9. The roughness values increased in the following order of surface treatment: Cleaning < CAA < FPL < PAA.

3.3 Bonding properties

The results of the single lap shear test are shown in Fig. 10. All coupons failed in cohesive failure mode, but the shear strength increased in the following order: Cleaning<FPL <CAA<PAA. The shear strengths after the salt spray test (5% NaCl, 200hr) are shown in Fig. 11. Only the cleaned coupons failed under the perfect adhesive failure mode, and they had nearly zero strength. The strength of the PAA and CAA coupons showed a slight decline and failed with the cohesive failure mode. The shear strength after hot-water immersion and hot-water/ice/thaw cycles are given in Figs. 12 and 13.

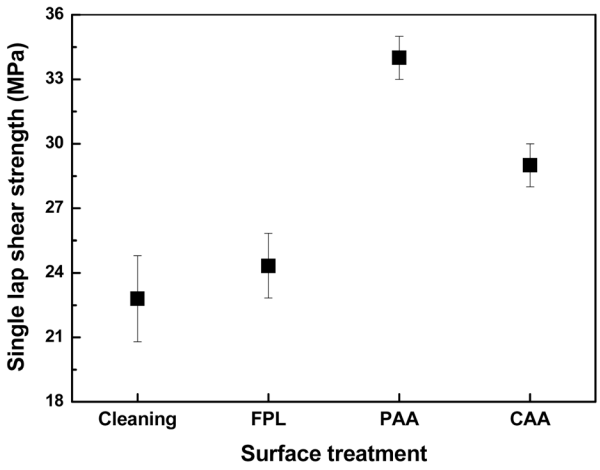

Fig. 10. Results of single lap-shear test

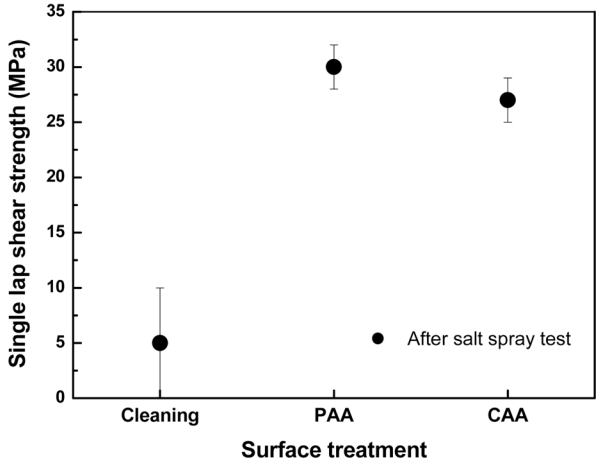

Fig. 11. Lap-shear strength after salt spray test for 200hr

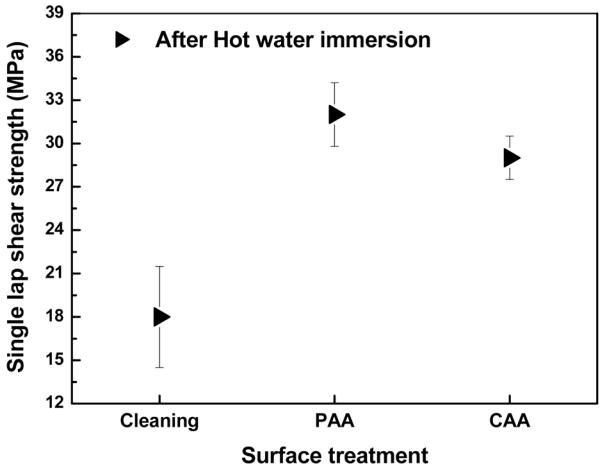

Fig. 12. Lap-shear strength after hot water immersion at 70 °C for 2 months

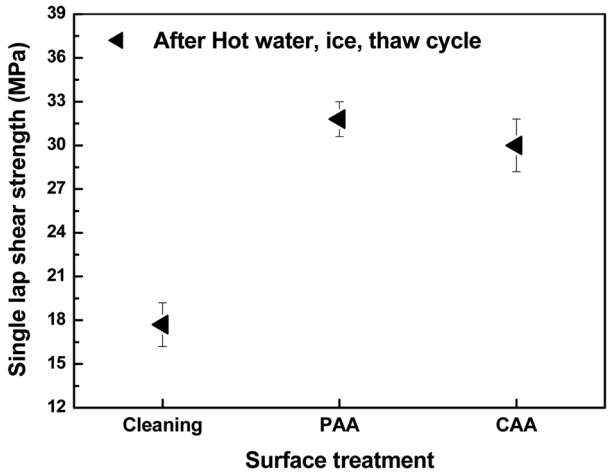

Fig. 13. Lap-shear strength after hot water-ice-thaw cycle for 2 months

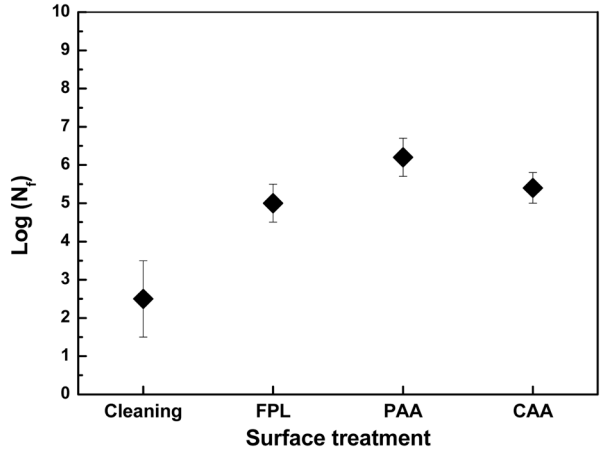

Fig. 14. Fatigue life of bonded samples by each pretreated aluminum alloy

The cleaned coupons failed under the partial cohesive failure mode, and the PAA and CAA coupons failed under the cohesive failure mode. After immersion in hot water and hot water/ice/thawing, the shear strength of the cleaned coupon decreased by about 5 MPa, and the PAA coupon decreased by about 2 MPa. However, the strength of the CAA coupon did not change. The fatigue test results are shown in Fig. 14. The fatigue life of the CAA coupons increased 800 times compared to the cleaned coupons, and the fatigue life of the PAA coupons increased 5,000 times compared to the cleaned coupons.

4. Conclusion

The experimental results on the influence of surface energy and topography in aluminum-to-aluminum bonding are as follows.

(1) The surface energy and work of adhesion of the aluminum alloy considering the correction factor were higher in the order of Cleaning <FPL <PAA <CAA. The polarity of the cleaned surface was almost zero, but after anodizing (CAA), the polarity had increased significantly.

(2) The macroscopic roughness of the surfaces of Cleaning, PAA and CAA was similar, but the microscopic roughness (scanning length=0.3 μm) increased in the order of Cleaning<CAA <FPL <PAA. The microscopic surface roughness of the PAA-treated sample was the highest.

(3) The lap-shear strength increased in the order of Cleaning<FPL <CAA <PAA. It can be seen that the bonding strength is most strongly influenced by the microscopic roughness of the adherend surface. This is because the larger the roughness, the larger the surface area and the larger the bonding area. The CAA treated surface showed good bond retention performance in harsh environments(hot water, salt spray, hot-water/ice/thawing cycle). This seems to have occurred because the CAA-treated surface energy and work of adhesion were the highest, taking into account the roughness correction factor, and also had good corrosion resistance.

(4) The fatigue test most clearly showed the different effect of each surface pretreatment on adhesion properties.

In conclusion, the microscopic roughness and surface energy of the aluminum alloy were the main factors influencing aluminum adhesion properties and durability.

REFERENCES

1. G. W. Critchlow, D. M. Brewis, *Int. J. Adhesion and Adhesives* **16**, 255 (1996).
2. A. J. Kinloch, M. S. G. Little, and J. F. Watts, *Acta materialia* **48**, 4543 (2000).
3. M. Kalnins, A. Sirmacs, and L. Malers, *Int. J. Adhesion and Adhesives* **17**, 365 (1997).
4. L. H. Lee, Adhesive Bonding, *Plenum Press*, 1, New York and London (1991).
5. G. Fourche, *Polymer Engineering and Science* **35**, 957

(1995).
6. K. W. Allen, *Int. J. Adhesion and Adhesives* **13**, 67 (1993).
7. W. Brockmann and O. D. Hennemann, *H. Kollek and C. Matz* **6**, 115 (1986).
8. A. J. Kinloch, *Adhesion and Adhesives, Science and Technology*, Chapter 3, Chapan and Hall, London, New York (1987).
9. G. V. Kuznetsov, E. G. Orlova, D. V. Feoktistov, A. G. Islamova, and A. V. Zhuikov, *Met. Mater. Int.* **26**, 46 (2020).
10. O. Lunder, B. Olsen, and K. Nisancioglu, *Int. J. Adhesion and Adhesives* **22**,143 (2002).
11. G. W. Critchlow, P. W. Webb, C. J. Tremlett, and K. Brown, *Int. J. Adhesion and Adhesives* **20**,113 (2000).
12. H. S. Kang, J. H. Lee, J. H. Park, H. A. Lee, W. I. Park, S. M. Kang, and S. C. Yi, *Korean J. Met. Mater.* **57**, 582 (2019).
13. Y. Zuo, P. H. Zhao, and J. M. Zhao, *Surface and Coating Technology* **166**, 237 (2003).
14. R. P. Digby and D. E. Packham, *Int. J. Adhesion and Adhesives* **15**, 61 (1995).
15. A. N. Rider and D. R. Arnott, *Int. J. Adhesion and Adhesives* **20**, 209 (2000).
16. Y. Park, H. Ji, and C. Jeong, *Korean J. Met. Mater.* **58**, 97 (2020).
17. K. Y. Rhee and J. H. Yang, *Composites Science and Technology* **63**, 33 (2003).
18. R. Broad, J. French, and J. Sauer, *Int. J. Adhesion and Adhesives* **19**, 193 (1999).
19. J. D. Eo, J. G. Kim., Y. S. Jung, J. H. Lee, and W. B. Kim, *Korean J. Met. Mater*. **59**, 73 (2021).
20. W. Brockmann, O. -D. Hennemann, H. Kollek, and C. Matz, *Int. J. Adhesion and Adhesives* **6**, 115 (1986).
21. J. W. Chin and J. P. Wightman, *Composites*: Part A **27A**, 419 (1996).
22. K. Uehara and M. Sakurai, *J. Materials Processing Technology* **127**, 178 (2002).
23. D. K. Kohli, *Adhesion & Adhesives* **19**, 213 (1999).
24. G. Xiao, *J. Colloid and Interface Science* **171**, 200 (1995).
25. S. J. Park, H. C. Kim, and H. Y. Kim, *J. Colloid and Interface Science* **255**, 145 (2002).
26. J. Lawrence, *Materials Science and Engineering* A00, 1 (2003).
27. M. J. J. Schmidt and L. Li, *Applied Surface Science*, **208**, 651 (2003).